BABES-BOLYAI UNIVERSITY

FACULTY OF PHYSICS

Emilia Sabina Vanea

Spectroscopic Studies on Aluminosilicate Biomaterials Containing Iron and Rare Earths

PhD Thesis Summary

Scientific Supervisor:

Prof. Dr. Viorica Simon

Cluj-Napoca

2010

Table of Contents

Introduction 3
1. Sample preparation 6
2. Sample characterization by XRD 6
3. Magnetic measurements 8
4. Sample characterization by EPR 10
5. Sample functionalization 13
5.1 Sample characterization by XPS and IR 13
5.1.1 XPS results received for $60SiO_2 \cdot 20Al_2O_3 \cdot 10Fe_2O_3 \cdot 10Y_2O_3$ system 13
5.1.2 FT-IR results received for $60SiO_2 \cdot 20Al_2O_3 \cdot 10Fe_2O_3 \cdot 10Y_2O_3$ system 19
5.1.3 XPS results received for $60SiO_2 \cdot 20Al_2O_3 \cdot 20Fe_2O_3$ system.....20
5.1.4 IR results received for $60SiO_2 \cdot 20Al_2O_3 \cdot 20Fe_2O_3$ system.....25
Conclusions 27
Selected References 29

Keywords*: sol-gel, aluminosilicates, radiation induced defects, EPR, nanostructured microparticle, protein adsorption, BSA, fibrinogen, SBF, XPS, FT-IR,*

Introduction

Biomaterials have a long-lasting history over more than several thousand years. Definitions of biomaterials and of biocompatibility have changed since that time with respect to the acquired knowledge and the increasing performance of a material. So a biomaterial must now be understood as a (living or not-living) *material destined to be put in contact with living tissues and/or with biological fluids to evaluate, treat, modify forms or replace any tissue, organ or function of the body* [1, 2].

The definition of biocompatibility has even more been changed with respect to the considered material. First defined for biological inert materials, it has been adapted to biological active and finally functionalized materials for drug binding and drug delivery. It also has to consider biodegradable and natural materials. Its today most objective definition should be *the property of a biomaterial that is to generate in the host an appropriate reaction* [2]. This means that knowing the multiple transient signals in the organism, it is utopia to want not to generate any unwanted reaction. Thus it is preferable to try to minimize it and to control it.

Glass systems are very often used as bone repairing and substituting materials in many dental and orthopedic applications due to their excellent biocompatibility and osteointegration [3].

Due to their high stability in the body, the aluminosilicate glass ceramics found several medical applications [4-7-10].

The aluminosilicate glass ceramics are highly stable in the body and by addition of iron oxide they could be optimised for hysteresis heating of interest in hyperthermia.

Hyperthermia has been gaining a lot of interest recently as a method for curing cancer especially as an adjunct to other modalities such as radiotherapy and chemotherapy. The simultaneous application of radiotherapy and hyperthermia considerably enhances the therapeutic effects of the two cancer treatment methods [11]. Hyperthermia is a heat treatment, the temperature of the tissue being artificially elevated in order to receive therapeutic benefits [12]. It is performed by generating of temperatures up to 45-47°C by the magnetic nanoparticles injected locally near the cancerous tissue, in the presence of an external magnetic field.

The most important results obtained studying these systems refers to structure-properties corelation and on effects of different external agents like temperature, nuclear radiations, chemical agents and mechanical stress on the physical-chemical caracteristics [3,8].

It is necessary to sterilize all medical implants after fabrication and prior to their use to reduce the risk of infections and associated complications [13, 14].

Despite the availability of a wide range of sterilisation techniques, it is generally agreed that no single sterilisation process is capable of sterilising without adverse effects, all processes having their own advantages and disadvantages [15-17]. An effective sterilization method must guarantee

the required sterility assurance level with a minimum effect on the chemical, physical and biological properties of the biomaterial [18, 19].

This study describes the gamma irradiation effects on aluminosilicate compounds of biomedical interest for sterilisation purpose. The paramagnetic defect centres in silica–based sol-gel materials were produced at room temperature. A promising technique that can be used to describe and explain the radiation-induced paramagnetic centres is the Electron Paramagnetic Resonance (EPR).

Magnetic particles for the hyperthermia/radiotherapy application have to be injected locally or intravenously at the site of the tumor. After the particles are injected into the bloodstream they are rapidly coated by components of the circulation, such as plasma proteins. On the other hand, foreign products are recognized by the body's major defence system, the reticulo-endothelial system (RES) and are quickly removed from blood circulation [20]. This process is known as opsonization.

A solution to this problem is to encapsulate the nanoparticles in a protein shell. The protein should be such that it should avoid detection by the RES and thus ensure longer sustenance of the particles within the body [21].

The role of the dense require surface modification, that would ensure particles were non-toxic, biocompatible and stable to the RES, is to inhibit opsonization, thereby permitting longer circulation times.

It is been widely accepted that the protein adsorption behaviour must be controlled to control a biomaterial surface and thus the study of protein-surface interaction should continue to be of central importance for biomaterial development.

We describe the adsorption characteristics of bovine serum albumin (BSA) and fibrinogen (Fg), two main plasma components and the relevant proteins adsorbed on the surface of blood contact biomaterials.

Albumin is the predominant plasma protein, making up 60-70% of plasma [22]. Albumin is generally considered to "passivate" the surface and greatly reduce the acute inflammatory response to the material [23]. Fibrinogen is the third primary plasma component and it immediately adsorbs to implanted biomaterials [24] being one of the most relevant proteins that are adsorbed on biomaterial surfaces because it takes part in blood coagulation, facilities adhesion and aggregation of platelets, which are very important properties in the processes of both haemostasis and thrombosis.

Thus another objective of this in vitro study was to functionalise the aluminosilicates compounds containing iron and yttrium/dysprosium in order to improve the systems biocompatibility. The proteins adsorption was investigated by means of XPS and FT-IR spectroscopy. X-ray Photoelectron Spectroscopy (XPS) is a very useful analysis tool dedicated to investigate the atomic composition and chemical environment of the outermost 2-10 nm layer of a

surface and can accurately determine the surface coverage. Transform Infrared Spectroscopy (FTIR) is one of the most used techniques for studying protein secondary structures.

The thesis begins with the present introduction and continues with five chapters each of them followed by references and finishes with conclusions.

The first chapter begins by a general definition of biomaterials and biocompatibility, and then introduces the basic structural unit of SiO_2 and its principal defects. It treaties also the main sterilisation techniques, together with the advantages of gamma sterilisation.

The second chapter describes hyperthermia for cancer treatment and the biological rationale for associating hyperthermia with radiation.

The third chapter approaches protein-surface interactions fundamentally responsible for the biocompatibility of the materials.

The fourth chapter contains a brief description of the experimental methods used both for preparation and analysis of the systems.

The last chapter describes the experimental results obtained for the aluminosilicates system containing iron and rare earth.

1. Sample preparation

The sol-gel method, via hydrolysis and condensation of molecular precursors, was chosen in this procedure to prepare aluminosilicate glasses doped with iron, yttrium and dysprosium content. The sol-gel approach is a high-purity process that leads to excellent homogeneity.

The composition of the prepared aluminosilicate system is given in the next table (Table 1).

Table 1. *Sample composition.*

Code	**Components (mol %)**				
	SiO_2	**Al_2O_3**	**Fe_2O_3**	**Dy_2O_3**	**Y_2O_3**
ASF	60	20	20		
ASFD	60	20	10	10	
ASFY	60	20	10		10

The compounds were thus synthesized by sol-gel method using as starting materials silicic acid ($Si(OH)_4$), aluminium nitrate ($Al(NO_3)_3 \cdot 9H_2O$), iron nitrate ($Fe(NO_3)_3 \cdot 9H_2O$), yttrium nitrate ($Y(NO_3)_3 \cdot 6H_2O$) and dysprosium nitrate ($Dy(NO_3)_3 \cdot H_2O$) with high grade of purity.

The calculated amount of precursors were dissolved in distilled water and mixed together at the 90°C in order to form a gel structure.

After the gel formation, the samples were filtrated, dried in an electric oven at 110ºC for couple of hours and then heat-treated at 500°C for one hour and 1200°C for 24 hours, respectively. The aim of the thermal treatment was to create iron oxide crystalline phases to heat by hysteresis.

Thermal treatment can also restore the device performance and/or relieve the damages induced after sample preparation. The annealing process alters the microstructures of a material and annihilates the defects, and can be accomplished by the diffusion of defects to the surface, the recombination of interstitials and vacancies, or the re-orientation of defects [25].

2. Sample characterization by XRD

The structure of prepared aluminosilicates compounds was investigated before and after applied thermal treatment at 500°C and 1200°C by X-ray Diffraction (XRD).

The X-ray diffraction analysis was carried out on a Shimadzu XRD-6000 diffractometer using CuK_α radiation (λ=1.54 Å), with Ni–filter.

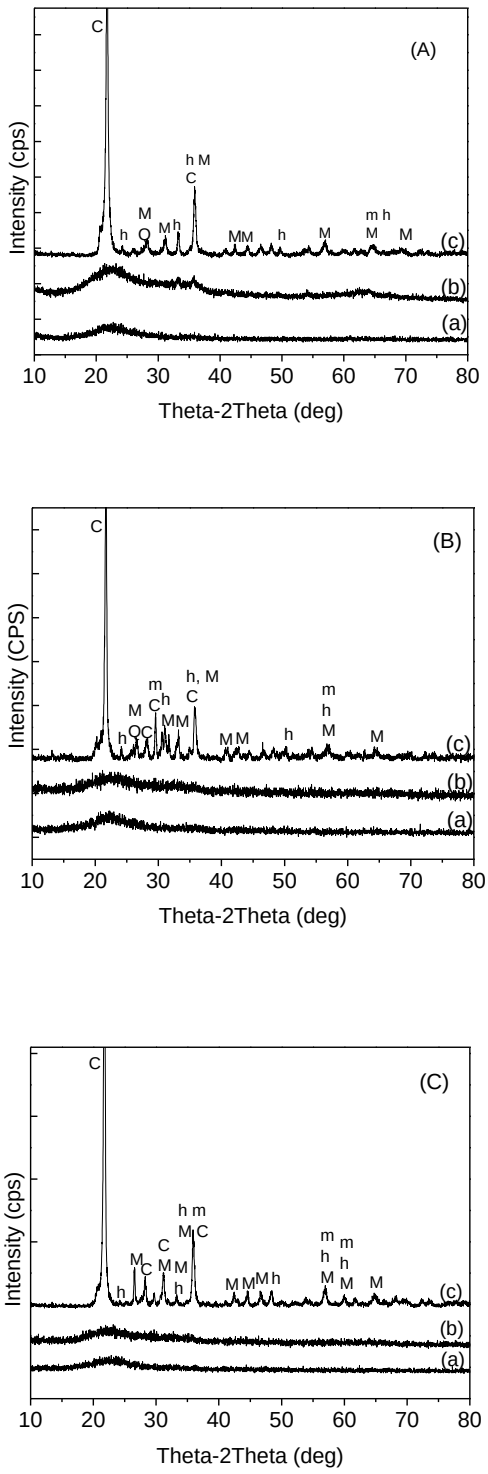

Figure 1. *XRD patterns of samples ASF (A), ASFD (B) and ASFY (C) before (a) and after heat-treatment at 500^{o}C (b) and 1200^{o}C (c).*

X-ray diffractograms show the amorphous structure before thermal treatment and an increasing crystalline structure after thermal treatment applied at 500°C and 1200°C, respectively as shown in images below.

The X-ray diffraction pattern of dried sample Figure 5.1 (A) reveals no crystalline. However, the peaks of the 500^{o}C sample are not well defined; the diffuse X-ray peaks indicate also the presence of poorly crystallized hematite particles.

The 1200°C heat treatment determines the development of SiO_2 cristobalite (C) and quartz (Q) [26], $Al_6Si_2O_{13}$ mullite (M) [27], Fe_2O_3 hematite (h) and Fe_3O_4 magnetite (m) [28] nanocrystals. Crystal sizes estimated with Scherrer equation according to the position and width of XRD peaks are up to 75 nm (Fig. 1).

3. Magnetic measurements

In order to establish the magnetic behavior of the synthesized samples was checked also the magnetic properties such as magnetic saturation and Curie temperature.

For the manipulation of magnetic particles, it is very important to know their magnetic moment. This was measured with the Alternating Gradient Magnetometer (AGM) MicroMag 2900 from the Princeton Measurement Corporation.

The magnetization measurements were carried out using a Curie-Weiss balance. The field dependence of magnetization was determined on home-made equipment for the systems thermal treated at 1200 °C.

The magnetic moment measurements as a function of magnetic field indicate a high magnetic moment values and a ferromagnetic behavior of the investigated sample (Fig. 2).

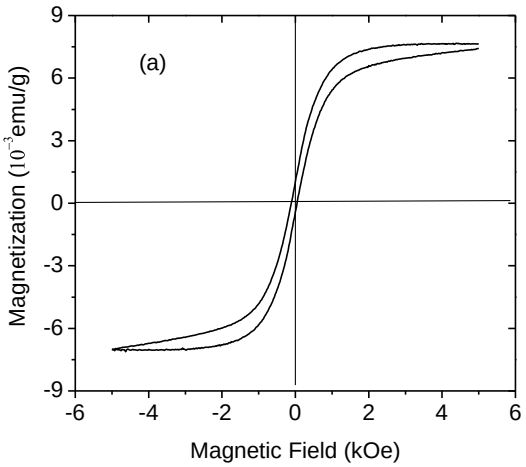

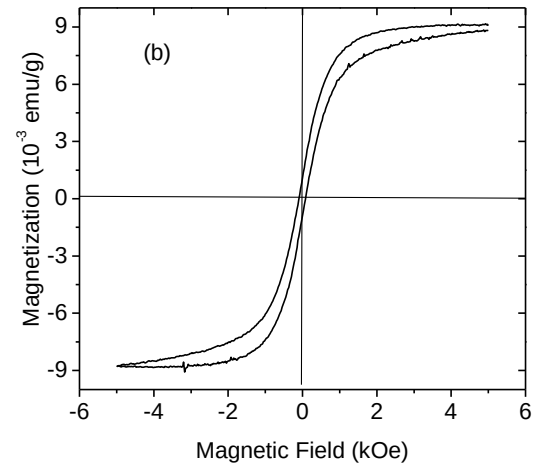

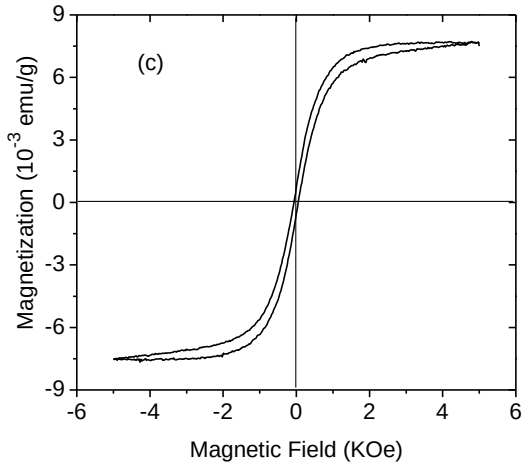

Figure 5.2 *Field dependence of magnetization for ASF (a), ASFY (b), ASFD (c) after applied thermal treatment at 1200 °C.*

The temperature dependence of the magnetization shows for the sample ASF, the Curie temperature to be around 430 K (Fig. 3 a) and for the sample with dysprosium content (ASFD) the Curie temperature is around 711 K (Fig. 3 b). Even though, the Curie temperatures were much higher than the desired optimum 315 K for hyperthermia application, the compounds have appropriate magnetic properties showing a stable ferromagnetic behaviour, being the subject of further investigations.

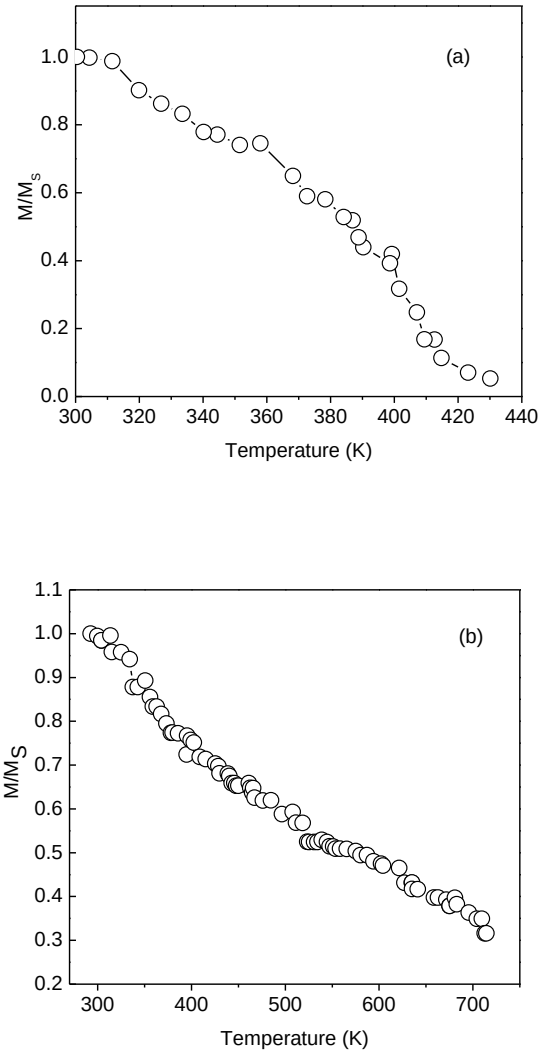

Figure 3. *Temperature dependence of normalised magnetisation for ASF (a) and ASFD (b) after applied thermal-treatment at 1200°C.*

4. Sample characterization by EPR

In order to use de samples as biomaterials they have to be sterilised to destroy the microorganisms and to reduce the risk of infections and associated complications.

Gamma sterilisation was chosen for this purpose being the most accessible technique. It is a simple, rapid and efficacious method of sterilisation. For this reason the samples were gamma irradiated and investigated with respect to possible occurrence of nocuous irradiation deffects.

The samples were thus exposed to gamma rays for a few weeks, using a ^{60}Co source with a debit dose of 10 Gy/h. The irradiation dose was close to 8 kGy.

Electron resonance spectra of the sol-gel materials were recorded by means of EPR spectrometer, ADANI type, operating at 9.4 GHz (X band). The magnetic field was modulated at 100 KHz. All spectra were recorded at room temperature.

The identified intrinsic point defects that are induced by radiation in SiO_2 include oxygen vacancy species such as E' centers (≡ Si•), non-bridging oxygen hole centre NBOHCs (≡ Si−O•), peroxy radicals (≡ Si−O−O•), and self-trapped holes (≡ Si −O• −Si ≡) [25].

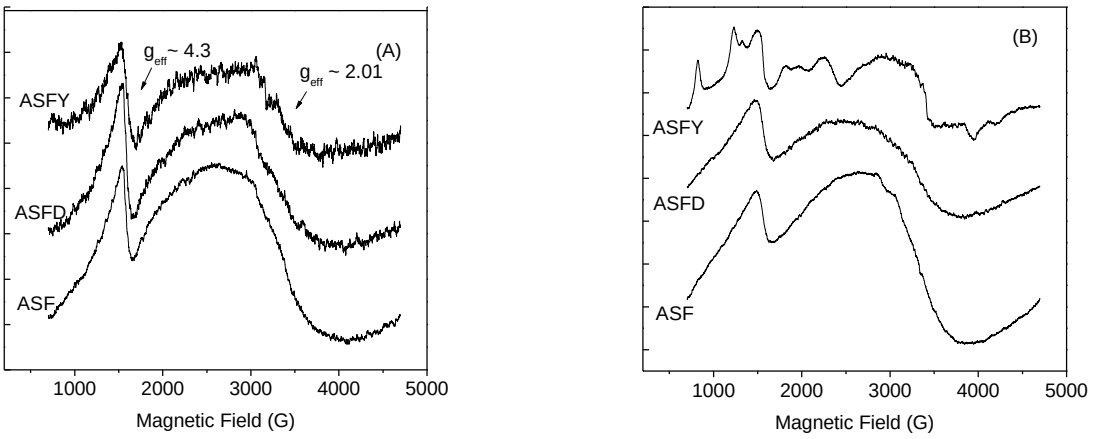

Figure 4. *Room temperature EPR spectra of aluminosilicate compounds thermal-treated at 500°C (A) and 1200 °C (B) before gamma exposure.*

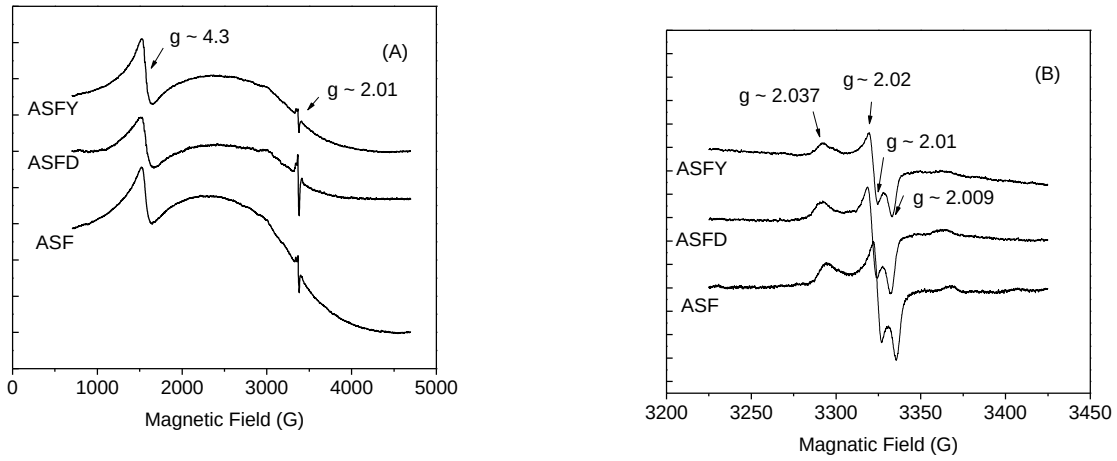

Figure 5. *Room temperature EPR derivate spectra of aluminosilicate compounds thermal-treated at 500°C, recorded using a sweep width of 4000 G (A) and 200 G (B) respectively.*

The EPR spectra recorded for non irradiated samples reveals only the lines corresponding to Fe^{3+} ions. The X-band EPR spectra of glasses with Fe^{3+} ions usually exhibit two well defined lines at $g_{eff} \approx 4.3$ corresponding to the isolated Fe^{3+} ion and at $g_{eff} \approx 2$ attributed to the Fe^{3+} species that participate to dipole-dipole interactions (Fig. 4) [29].

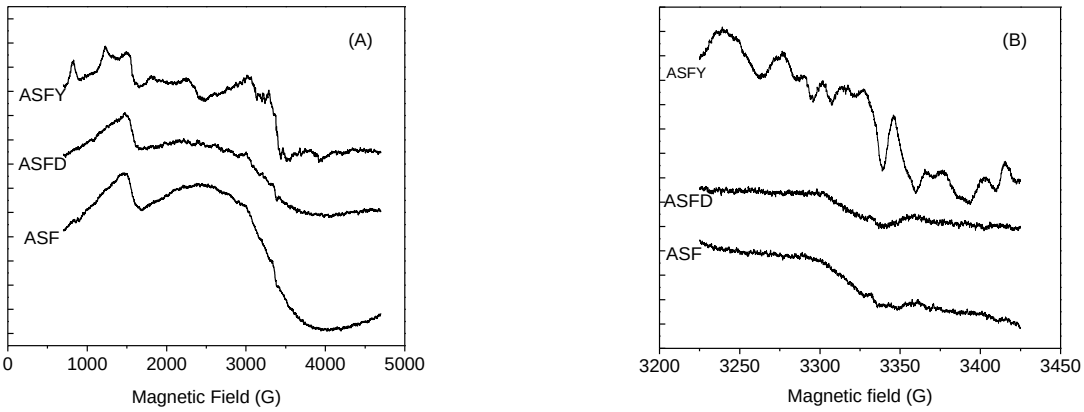

Figure 6. *Room temperature EPR derivate spectra of aluminosilicate compounds heat-treated at 1200°C, recorded using a sweep width of 4000 G (A) and 200 G (B) respectively.*

The EPR spectra for irradiated systems present additional signals occurring from paramagnetic defects, mainly detected for 500°C thermal-treated systems (Fig. 5 (A, B)).

Regarding the g factors of the resonance line received for the samples thermal-treated at 500°C, the presence of resonance line with $g \approx 2.037$ indicates the presence of paramagnetic peroxy-centres, OHC. The resonance line with $g \approx 2.02$, $g \approx 2.0179$, $g \approx 2.009$ can be assumed to NBOHC (Fig. 5 B) [30].

For the crystallised samples resulted after the thermal-treated applied at 1200°C (Fig. 6 (A, B)) the EPR spectra reveal a very weak signal at $g_{eff} \approx 2.01$ due to a low number of lattice defects associated with oxygen or cation vacancies, that denotes a very good stability of the crystalline compounds. The analysis indicates that for the samples treated at 500°C the defects concentration is meaningful greater than for the samples treated at 1200°C which is in very good agreement with the idea that thermal treatment can restore the material structure, and the native defect centres are almost vanished.

5. Sample functionalization

Thus, protein adsorption experiments were carried out by incubating the aluminosilicates sample containing iron and yttrium oxide in fibrinogen (Fg) solutions prepared in phosphate – buffered saline solution (PBS), and then the powder samples were immersed in simulated body fluid (SBF) enriched with bovine serum albumin (BSA).

The yttrium containing samples immersed in simulated biologic media were kept at 37°C in incubator for 5 minutes, 2 hours and 24 hours, under static conditions.

Aluminosilicate sample with $60SiO_2 \cdot 20Al_2O_3 \cdot 20Fe_2O_3$ after fine grinding was immersed in simulated body fluid (SBF) and also in simulated body fluid enriched with bovine serum albumin (BSA) in two different concentrations obtained by adding 3.33 and 6.67 g lyophilised BSA to 1 ℓ SBF. The system was kept also in the same incubator at 37°C, for 24 hours, 3 and respectively 7 days.

5.1 Sample characterization by XPS and IR

Surface chemical functionalization was determined by XPS and FT-IR spectroscopy.

XPS measurements were peformed using a SPECS PHOIBOS 150 MCD system equipped with monochromatic AlK α source.

Infrared spectroscopy has been used in this study to assess the conformational state of proteins adsorbed on aluminosilicates surface.

FTIR spectra of surface bound protein, before and after incubation, were conducted with attenuated total reflectance using Equinox 55 Bruker instrument in the range 4000-650 cm^{-1}, with a resolution of 2 cm^{-1}.

As the surface has been washed with analytically pure water, the protein left on the surface is considered to be irreversibly bound.

5.1.1 XPS results received for $60SiO_2 \cdot 20Al_2O_3 \cdot 10Fe_2O_3 \cdot 10Y_2O_3$ system

In the XPS survey spectrum recorded before immersion, only photoelectron peaks corresponding to the elements entering in the sample composition occur, excepting the C 1s photoelectron peak (Fig. 5.10). Carbon adsorption usually takes place on all surfaces exposed to the atmosphere and is immediately detected by the XPS technique.

As expected Y 3p, Fe 2p, Si 2p Al 2p peaks were found for all aluminosilicate-investigated samples (Fig. 7 (A, B)). However, for the protein functionalised substrates, detection of these four elements was less obvious due to the outer layer of protein (Table 2, 3). Similar results were obtained for the two types of proteins (BSA/Fg) used for functionalisation purpose.

Table 2. *Relative percentage of the main components before and after immersion in SBF/BSA solutions determined from survey spectra.*

Immersion time	**Elemental composition (at %)**						
	C	**N**	**O**	**Al**	**Si**	**Fe**	**Y**
0	6.92	-	53.08	2.3	36.77	0.18	0.75
5 min	28.43	5.68	37.7	2.19	25.47	0.04	0.49
2 hr	28.93	6.46	37.21	1.71	25.2	0.03	0.46
24 hr	33.21	6.67	35.16	1.54	23	-	0.42

Table 3. *Relative percentage of the main components before and after immersion in PBS/Fg solutions determined from survey spectra.*

Immersion time	**Elemental composition (at %)**						
	C	**N**	**O**	**Al**	**Si**	**Fe**	**Y**
0	6.92	-	53.08	2.3	36.77	0.18	0.75
5 min	43.11	10.69	29.26	0.8	15.96	0.02	0.16
2 hr	51.81	11.5	23.25	0.41	13.02	0.01	-
24 hr	48.53	13.52	27.83	0.1	10.02	-	-

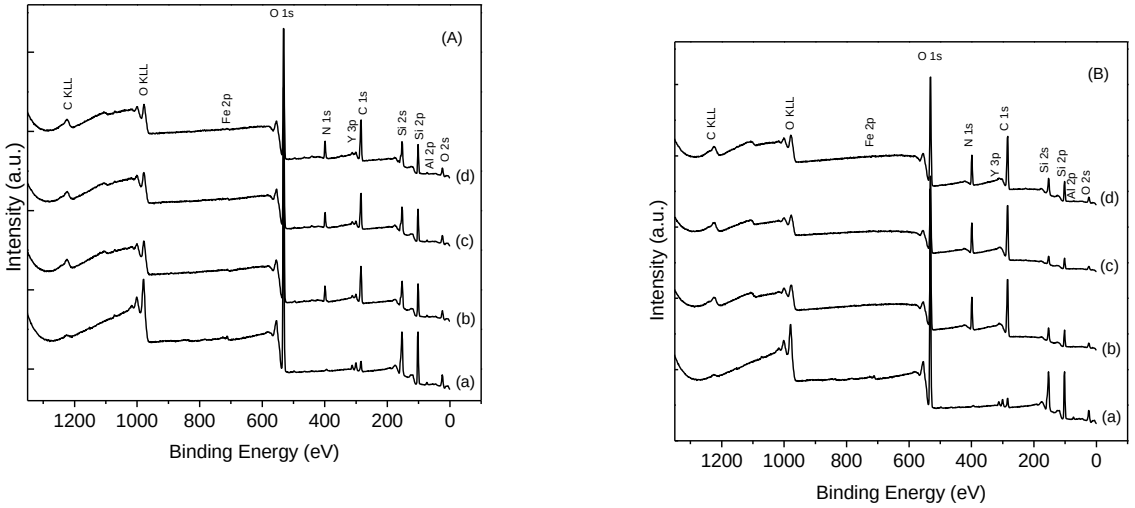

Figure 7. *XPS survey spectra before immersion (a), after 5 minutes (b), 2 hours (c) and 24 hours (d) immersion in SBF/BSA (A) and PBS/Fg (B) solutions.*

At the same time, analysis of the survey spectra indicates N 1s peaks occurring from the nitrogen present in every amino acid of the protein.

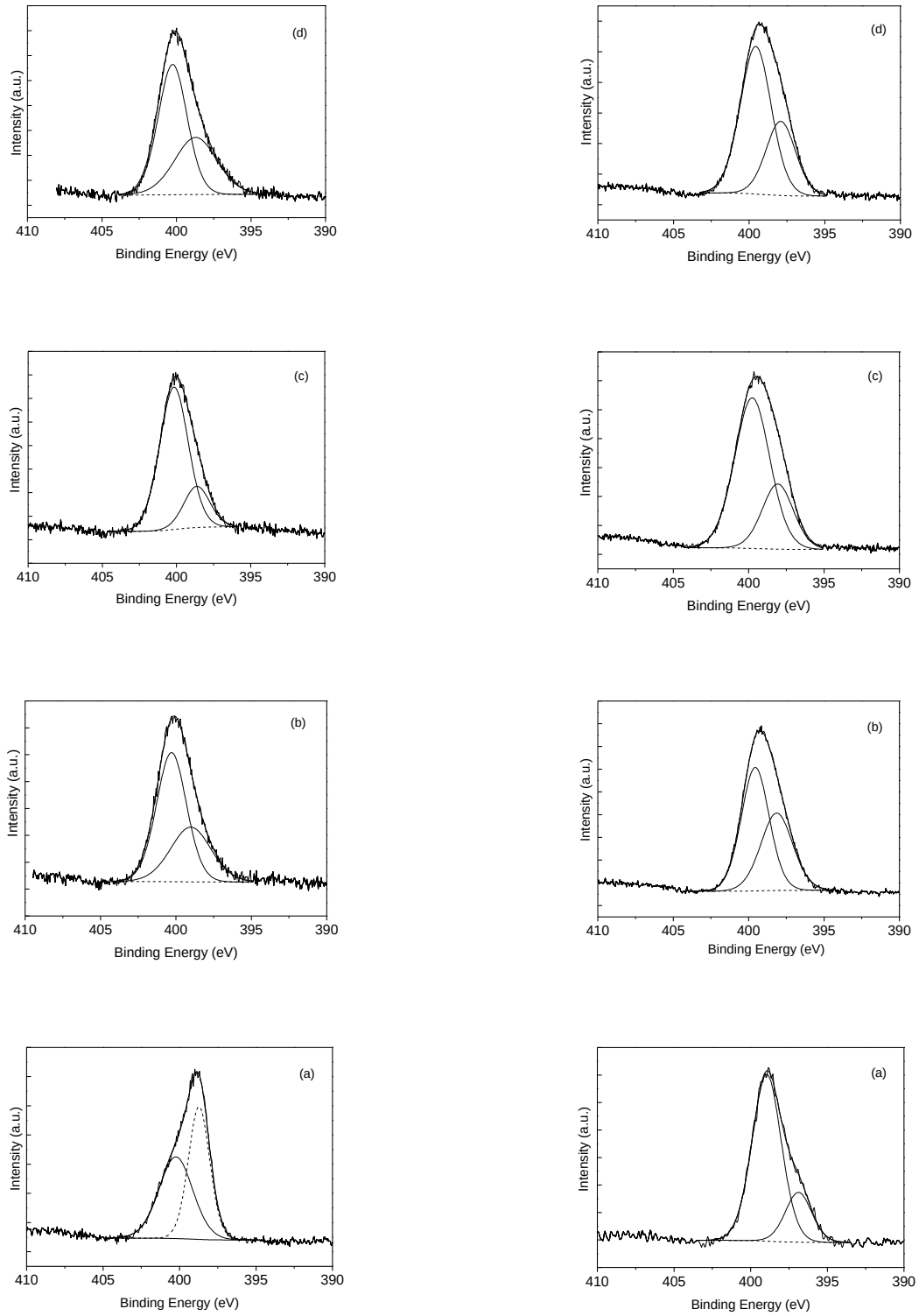

(A) (B)

Figure 8. *Deconvoluted N 1s high resolution XPS spectra of lyophilised BSA/Fg (a) and after 5 minutes (b), 2 hours (c) and 24 hours (d) immersion in SBF/BSA (A) and PBS/Fg (B) solutions.*

XPS measurements of the nitrogen concentration can be interpreted as an indirect measure of the protein content [31]. The nitrogen concentration was practically zero before the immersion of the sample in the protein solutions (Table 2, 3), that means it can be used as a reliable marker for protein adsorption, and N:C ratio is typically used as indicators of protein deposition [32].

The deconvolution of N 1s core level spectra (Fig. 8) reveals two components, centred at 398.2 and 400 eV, characteristic of C-NH_2 groups [33]. Actually, the N 1s photoelectron peaks recorded close to 400 eV are typical for nitrogen in organic matrix [34].

XPS analysis confirms the increase of N content after different incubation periods, larger sized protein will produce a higher nitrogen signal than a smaller sized protein. This is because the larger protein molecule has more nitrogen atoms in XPS sampling depth.

After sample immersion in protein solution the C 1s high-resolution spectra (Fig. 9) appear broader and signalise new type of bonds.

The C 1s photoelectron peaks were decomposed according to binding energies of carbon bonds in proteins. They are well fitted (Fig. 9) with components at 284.6 eV, corresponding to C-C and C-H bonds, 286.5 eV, corresponding to C-O bonds, and the component at 288.3 eV, corresponding to C=O bonds [34]. These are characteristic carbon bonds in proteins.

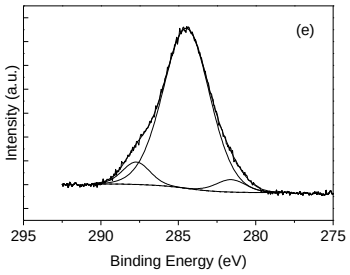

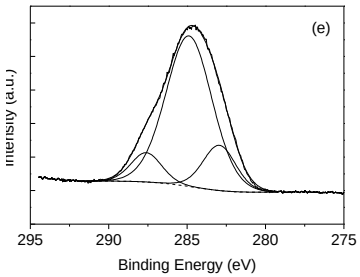

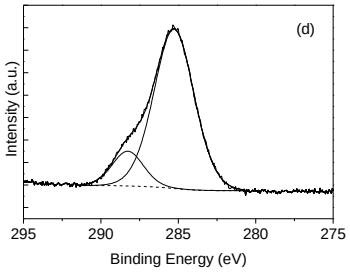

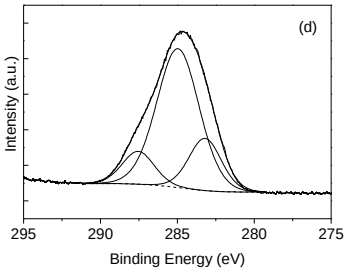

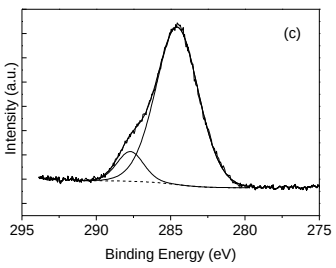

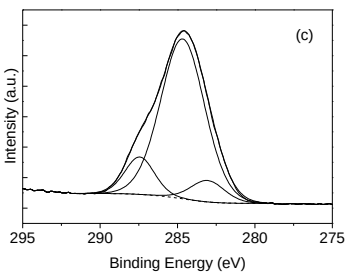

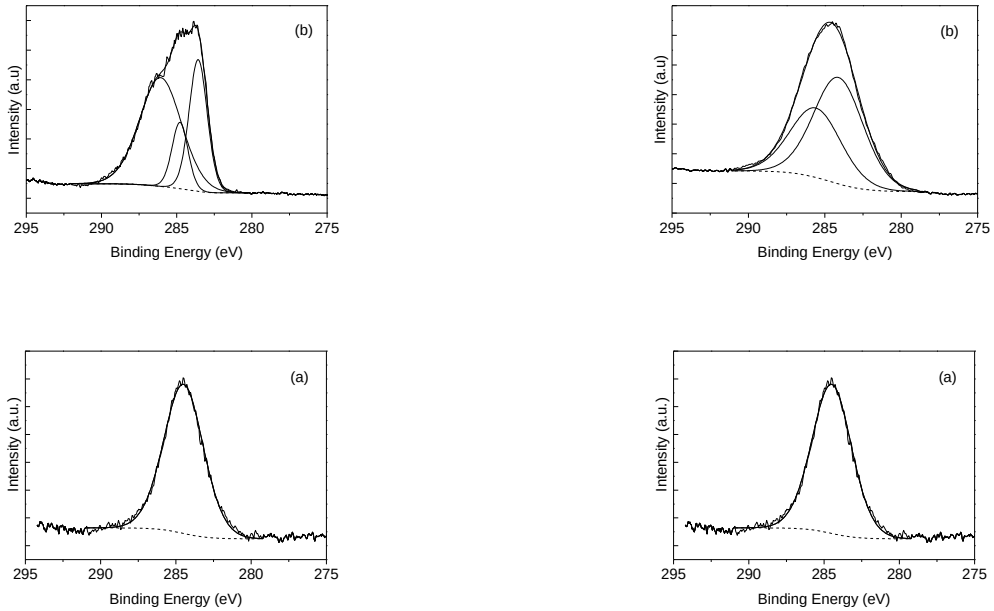

Figure 9. *Deconvoluted C 1s high resolution XPS spectra before immersion (a), of lyophilised BSA and Fg (b), and after 5 minutes (c), 2 hours (d) and 24 hours (e) immersion in SBF/BSA (A) and PBS/Fg (B) solutions.*

The O 1s signal before immersion in protein solution consists of a dominant component at 533.2 eV associated to Si-O-Si, and a second component at lower binding energy 531.5 eV, which are related to bridging oxygens (BO) and, respectively, non-bridging oxygens (NBO) occurring in the structural units of the aluminosilicate microparticles [37]. Based on the preponderance of BO relative to NBO in the nanostructurated aluminosilicate microparticles (Fig. 10 a), they are expected to own a high stability in the biological media.

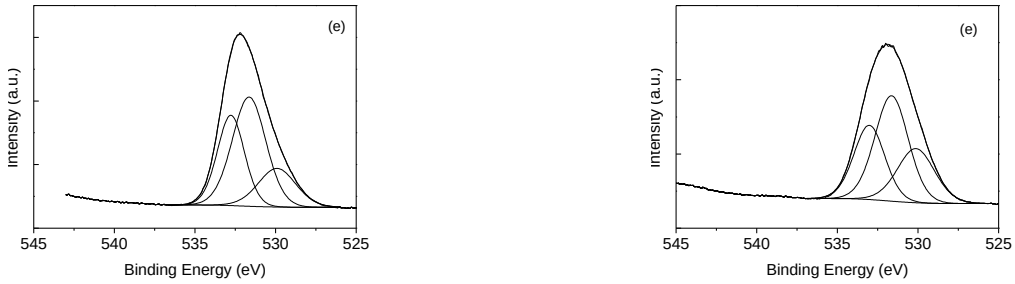

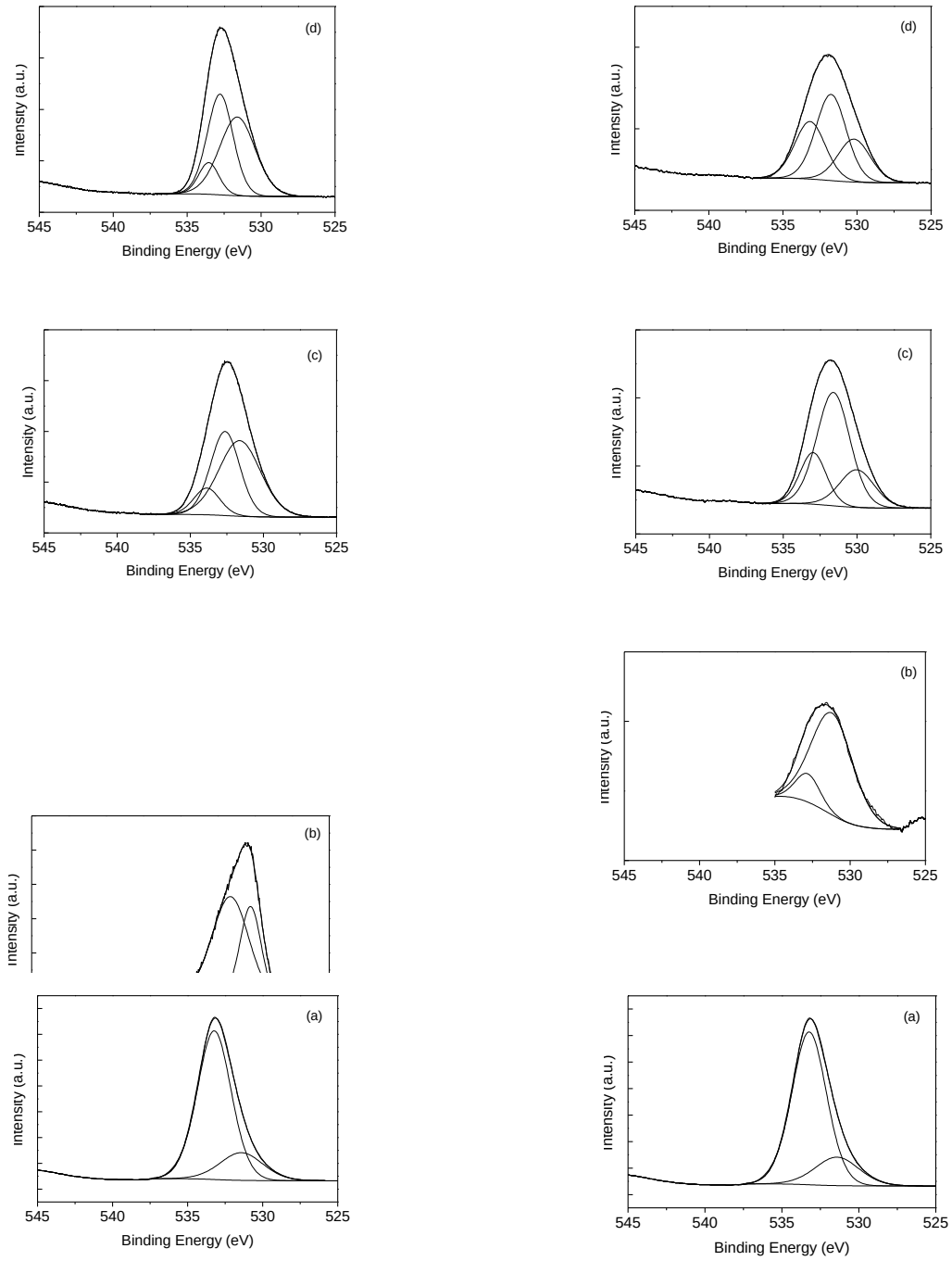

(A) (B)

Figure 10. *Deconvoluted O 1s high resolution XPS spectra before immersion (a) of lyophilised BSA/Fg (b), and after 5 minutes (c), 2 hours (d) and 24 hours (e) immersion in SBF/BSA (A) and PBS/Fg (B) solutions.*

After immersion in protein solutions, the O 1s photoelectron peaks are evidently broader and shifted to lower binding energies, mainly on the account of the BSA component located at 530.3, respectively of fibrinogen component located at 531.2 (Fig. 10 b).

The results obtained by deconvolution of O 1s photoelectron peaks suggest that the O 1s photoelectrons correspond significantly to peptidic oxygen of proteins [38].

5.1.2 FT-IR results received for $60SiO_2 \cdot 20Al_2O_3 \cdot 10Fe_2O_3 \cdot 10Y_2O_3$ system

The infrared spectroscopy results were analysed with respect to protein secondary structure. The proteins exhibit characteristic bands, emerging from vibration in the peptide linkages, in 4000-1200 cm^{-1} spectral range of FTIR spectra. There are three dominant bands, namely amide I band (1600-1700 cm^{-1}) which comprises contribution from 80% C=O stretching mode, Amide II (1500–1600 cm^{-1}: 60% N–H bending and 40% C–N stretching modes) and Amide III (1200–1330 cm^{-1}: 40% C–N stretching and 30% N–H bending modes) [39, 40]. The amide I band is mostly used to extract information about the secondary structure. Because each of the different secondary structural elements contributes to the FTIR spectrum, the observed amide bands are composed of several overlapping components representing helices, β-structures, turns and random structures.

The exact frequency of the amide I vibration depends on the nature of the hydrogen bonding involving C=O and N-H groups, this in turn is determined by the particular secondary structure adopted by the protein [41, 42, 43]. Band deconvolution using the second derivative can be used to identify the number and the position of the bands underlying the amides envelops [44].

Protein adsorption was evaluated for the two hours immersed system in SBF/BSA and PBS/Fg solutions.

Compared to the lyophilised BSA, there are several conformation changes for the protein adsorbed on surface (Fig. 11) toward a higher β-sheet/β-turn ratio, which indicates protein-surface interaction and enhanced blood compatibility [45].

Fibrinogen adsorbed on material surface also changes its native structure.The α-helix content of adsorbed fibrinogen obviously decreases and is mainly transformed to β-sheet which meaningfully increases, while the β-turn is less changed.

The β-sheet/β-turns ratio used to indicate the biocompatibility of the biomaterial shows that this ratio exhibits a higher value for the adsorbed protein compared to the native one (Fig. 10), indicating a good biocompatibility of the material, as supported by other data in literature [3].

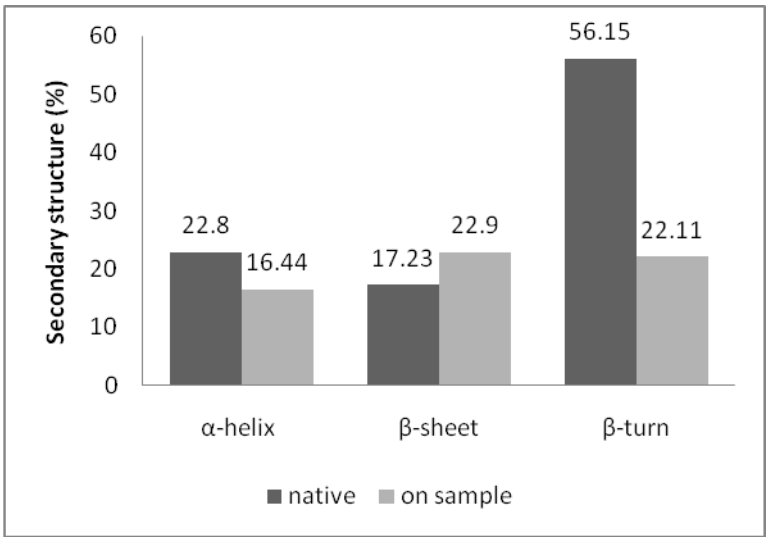

***Figure 11**. Distribution of secondary structures in bovine serum albumin.*

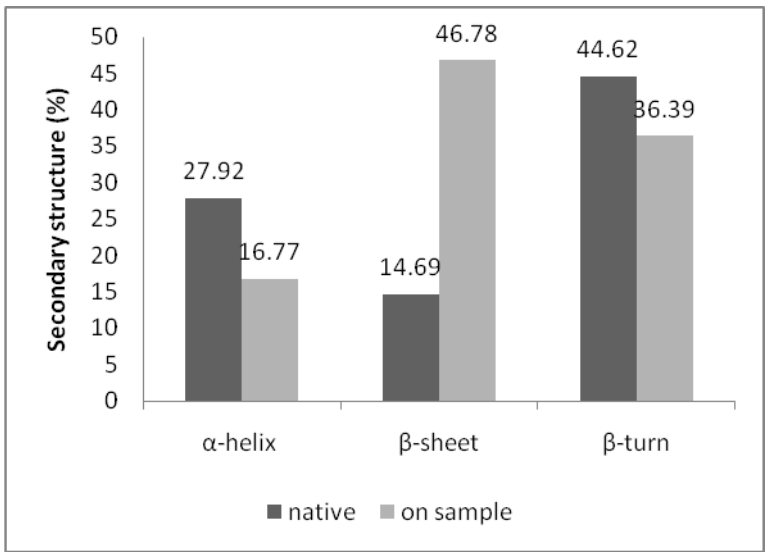

***Figure 12.** Distribution of secondary structures in fibrinogen.*

5.1.3 XPS results received for $60SiO_2 \cdot 20Al_2O_3 \cdot 20Fe_2O_3$ system

The uptake of proteins from solutions with different BSA concentration and prolonged immersion time was tested for the 20 % iron containing aluminosilicate system.

The occurrence of nitrogen species is clearly evidenced only after immersion in SBF with BSA solution (Fig. 13 c). In order to evaluate the uptake of protein on samples surface both survey and the C 1s, N 1s and O 1s core level spectra were examined.

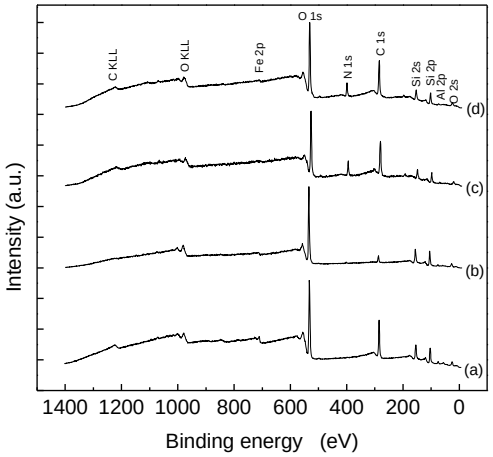

Figure 13. *Widescan XPS spectra before immersion (a), and after one day immersion in SBF (b), SBF enriched with BSA (c) and SBF twice enriched with BSA.*

The relative percentage of C, N and O after immersion in SBF solutions, determined from survey XPS spectra (Table 4) points out very close values for both concentrations of BSA in SBF, denoting that the attachment of the protein on the surface of the aluminosilicate sample is saturated even by immersion in the solution with lower BSA content.

Table 4. *Relative percentage of C, N and O after immersion in SBF solutions, determined from survey XPS spectra.*

BSA concentration in SBF (g/ℓ)	**Elemental composition (at %)**		
	C	**N**	**O**
0	19	-	81
3.33	52	11	37
6.67	51	10	39

The C 1s high resolution spectra recorded from the samples immersed in SBF/BSA solution (Fig. 14) contains the BSA signature after one day soaking in the SBF solution with low BSA content.

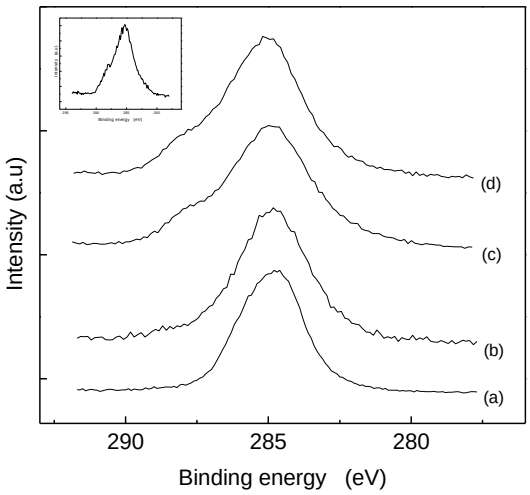

Figure 14. *C1s high- resolution XPS spectra before immersion (a), and after one day immersion in SBF (b), SBF enriched with BSA (c) and SBF twice enriched with BSA. In inlay is shown the spectrum recorded from lyophilized BSA.*

The deconvoluted C 1s photoelectron peaks (Fig. 15) provide more information. From the non-immersed sample only one single C 1s peak at 285.5 eV is recorded. Also after one day immersion in SBF the C 1s photoelectron peak is well fitted with a single line centered at 285.5 eV, but the peak is broadened, with 2.9 eV full width at half maximum (Fig. 15 b), while the full width at half maximum for the non-immersed sample (Fig. 15 a) is only 2.3 eV. The deconvolution of C 1s photoelectron peaks for the samples immersed in SBF solution enriched with BSA leads beside the peak at 285.5 eV to other two components centered at 286.7 and 288.6 eV, but their relative peak areas are notably different (Table 5). It is beyond doubt that the increased contribution of higher binding energy components is arising from the BSA adhered to the surface of aluminosilicate samples.

The N 1s photoelectron peak was recorded only for the samples immersed in SBF with BSA solutions (Fig. 16). The deconvolution of the peaks leads to different contributions for the two components centered at 400.3 eV and 399.1 eV. The binding energies of N 1s typical for organic matrices are close to 400 eV, related to C-N bonds [50]. The atomic percent estimated for nitrogen (8.6 %) is in good agreement with the values reported on the surface of silicon wafers after BSA adsorption [49].

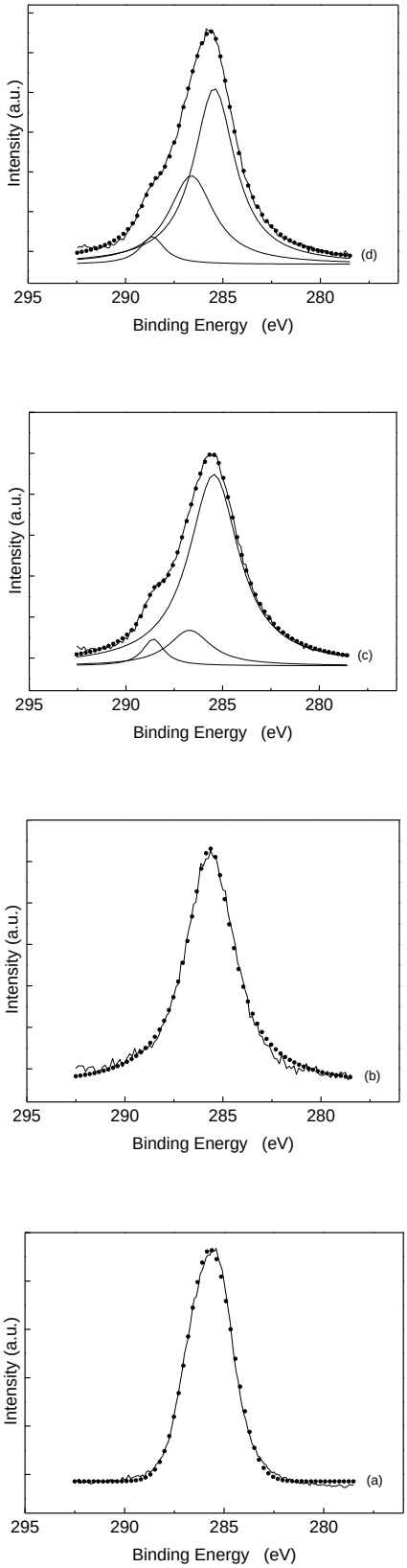

Figure 15. *Deconvoluted C 1s high resolution XPS spectra before immersion (a), and after one day immersion in SBF (b), SBF enriched with BSA (c) and SBF twice enriched with BSA (d).*

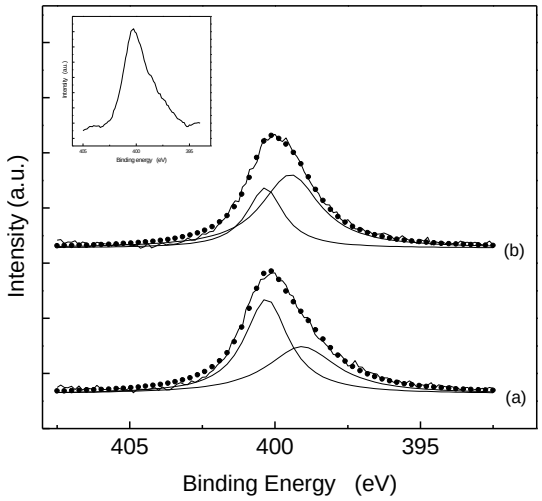

Figure 16. *C1s high-resolution XPS spectra before immersion (a), and after one day immersion in SBF (b), SBF enriched with BSA (c) and SBF twice enriched with BSA.*

In inlay is shown the spectrum recorded from lyophilized BSA.

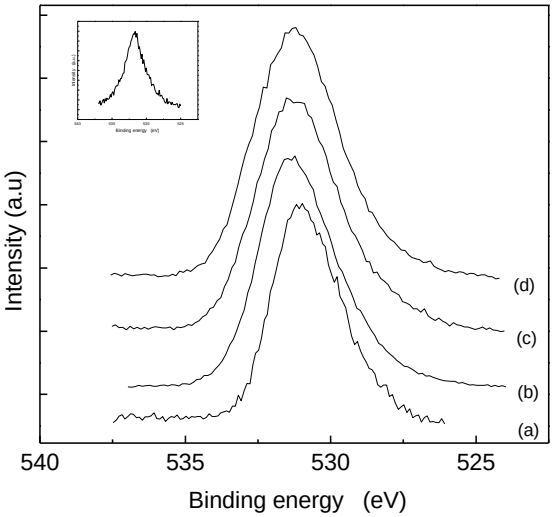

Figure 17. *O1s high-resolution XPS spectra before immersion (a), and after one day immersion in SBF (b), SBF enriched with BSA (c) and SBF twice enriched with BSA.*

In inlay is shown the spectrum recorded from lyophilized BSA.

With respect to the evolution of O 1s core level spectra (Fig. 5.28) one remarks symmetric peaks that are well fitted with a single line, that overlaps the contributions due to the oxygen atoms

from the aluminosilicate sample surface, adsorbed –OH groups and peptidic oxygen of BSA [38]. The full width at half maximum of O 1s photoelectron peak recorded from the non-immersed sample is 2.3 eV and increases to 2.7 eV after immersion in pure SBF and to 2.9 eV after immersion in BSA-SBF, as well in 3.33 and 6.67 g BSA /1 ℓ SBF solution; the broadening of the full width at half maximum points out a larger distribution of the oxygen sites.

5.1.4 IR results received for $60SiO_2 \cdot 20Al_2O_3 \cdot 20Fe_2O_3$ system

The features of FTIR spectrum recorded from lyophilised BSA introduced into simulated body fluid it is well evidenced in the FTIR spectrum of the sample immersed for seven days in the solution containing 6.67 g BSA / ℓ SBF. The deconvolution of amide I absorption band of lyophilized BSA and of adsorbed BSA on the aluminosilicate sample is presented in Figures 18 A, B, respectively.

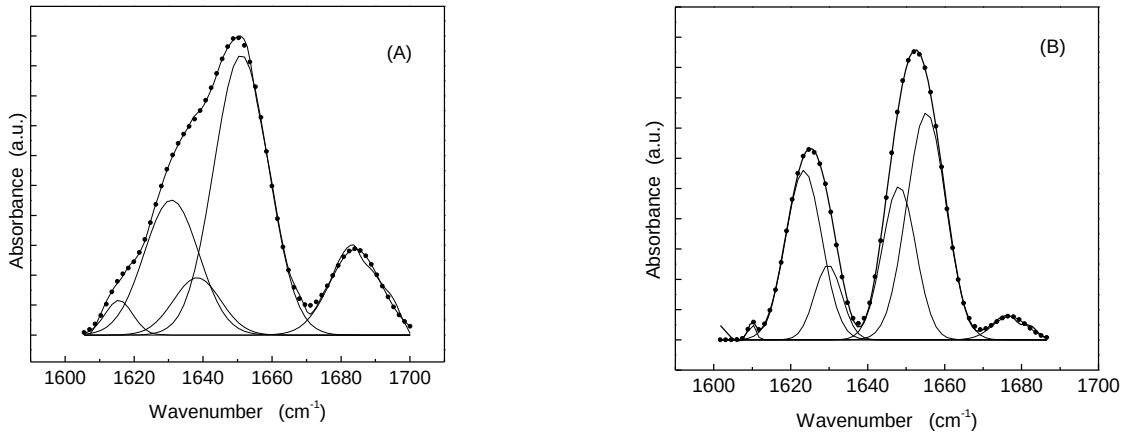

Figura 18. *Deconvolution of amide I absorption band of lyophilized BSA (A) and adsorbed BSA on aluminosilicate biomaterial (B).*

Deconvolution of the native albumin amide I band was made assuming five components, while for the adsorbed albumin six components are considered. The recent literature [44] regarding a curve fitting procedure shows that six or five components had to be used for hydrophilic or hydrophobic surfaces, respectively. The occurrence of a new band around 1610 cm^{-1} is assignable to the intermolecular β-sheet structure (or side chain) which is indicative for the aggregation of the protein. One can observe from the data summarised in Fig. 19 that β-sheet content increases from 27.1 % in lyophilized state to 34.7 % after adsorption, as well as the random conformation from 8.8

% to 18 %. In the same time α-helix conformation decreases from 49.7 % to 42 % after adsorption and the turns from 14.4 % to 4.3 %.

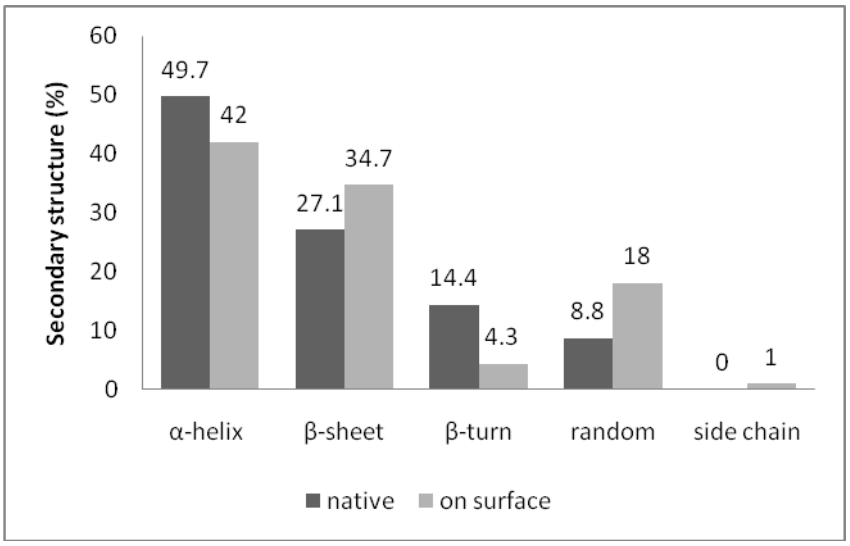

Figure 19. *Distribution of secondary structures in bovine serum albumin.*

In our measurements, β-sheet/ β-turns ratio exhibit a higher value for the adsorbed protein compared to the native one, indicating a good biocompatibility of the material, as supported by other data in literature [44].

BSA adsorption was confirmed by infrared data. XPS spectroscopy clearly appears more sensitive than FTIR performed in reflectance mode to the changes occurred on the sample surface after immersion in simulated body fluids [49, 50].

Conclusions

- Homogenous aluminosilicate systems containing iron and rare earths (yttrium and dysprosium) were prepared following the sol-gel route.
- After thermal treatment, the iron preponderantly crystallises as magnetite, but hematite and maghemite are also developed, expecting a ferromagnetic behaviour. The developed crystallites are nanosized.
- Magnetic moment measurements as a function of magnetic field approve the expected ferromagnetic behaviour.
- The temperature dependence of the magnetization shows for ASF and ASFD samples the Curie temperature close to 430 K and 711 K, respectively.
- After gamma exposure of samples, oxygen hole centres (NBOHC) and peroxy centres were evidenced by EPR spectroscopy.
- It was evidenced that paramagnetic defects may occur during preparation and can be induced by gamma exposure, but they disappear while the thermal treatment temperature increases, denoting that the greater the crystallisation degree the better the stability of the irradiated samples against the occurrence of structure defects.
- First evidence of microparticles interaction with the protein is the occurrence in the XPS spectra of N 1s photoelectron signal with increasing intensity during the incubation period from 5 minutes to 24 hours, and the significant percentage reduction of the elements entering in the composition of the pristine samples.
- The nitrogen content established already after 5 minutes immersion time indicates the quick attachment of BSA and fibrinogen onto the microparticles surface.
- After sample incubation in protein solution, the C 1s core level spectra contain components of binding energies characteristic for peptidic carbons.
- The O 1s signal before immersion in protein solution are related to bridging oxygens (BO) and non-bridging oxygens (NBO) occurring in the structural units of the aluminosilicate microparticles.
- The preponderance of BO relative to NBO in these samples supports the expectation of a high stability in the biological media.
- After immersion in protein solutions, the O 1s photoelectrons correspond significantly to peptidic oxygen of proteins.
- Diminished oxygen content is detected on the microparticles surface for increasing immersion periods, because after incubation in protein solutions the aluminosilicate sample, initially with

high oxygen content, offers as outmost layer the attached BSA or fibrinogen protein of lower oxygen content.

- The protein concentration in SBF influences the building up of the BSA layer, but after short immersion periods the surface is nearly saturated in taking up BSA functional groups regardless of BSA concentration in SBF.
- The analysis of FTIR absorption bands characteristic for secondary structure of proteins shows that the β-sheet/β-turns ratio exhibits a higher value for the adsorbed proteins compared to the native ones, which indicates a good biocompatibility of these materials.
- The attachment of BSA/fibrinogen is proved by the β-sheet structure of amide I at 1650 cm^{-1} and spectral changes around 1540 cm^{-1}, assigned to amide II and 1320 cm^{-1}, assigned to amide III.
- The results of this study provide evidences that the synthesis of aluminosilicate nanostructured microparticles containing iron and yttrium/dysprosium can be useful in potential applications of simultaneous radiotherapy and hyperthermia.

Selected References

[1]. S.V. Bhat, Biomaterials, Alpha Science, Harrow U.K. 2005.

[2]. H. F. Hildebrand, N. Blanchemain1, G. Mayer, Y. M. Zhang, O. Melnyk, M. Morcellet and B. Marte, Key Engineering Materials Vols. 288-289, 47-50, 2005.

[3]. I. D. Xynos, A. I. Edgar, L. D. K. Buttery, L. L. Hench, J. M. Polak, J. Biomed. Mater. Res, 55, 151, 2001.

[4]. L.L. Hench, D.E. Day, W. Holand, V.M. Rheinberger, Glass and Medicine**,** Int J Appl Glass Sci; 1:104–117, 2010.

[5]. D. Day, Am Ceram Soc Bull; 74: 64-68, 1995.

[6]. J.K. Bibby, N.L. Bubb, D.J. Wood, P.M. Mummery, J Mater Sci: Mater Med; 16:379– 385, 2005.

[7]. V. Simon, D. Eniu, A. Gritco, S. Simon, J Optoelectr Adv Mater ; 9: 3368-337, 1, 2007.

[8]. R.F. Brown, L.C. Lindesmith, D.E. Day, Int. J. Rad. Appl. Instrum B, 18, 783, 1991.

[9]. S.W. Lee, W.D. Reece, Phys. Med. Biol., 50, 151, 2005.

[10]. J.E. White, D.E. Day, Key Eng. Mat., 94-95, 181, 1994.

[11]. M. Kawashita, H. Takaoka, T. Kokubo, T. Yao, S. Hamada, T. Shinjo, J. Ceram. Soc. Jpn., 109, 39, 2001.

[12]. S. K. Alpard et al, Therapeutic hyperthermia, Perfusion, 11, 425-435, 1996.

[13]. J. M. Anderson, B. Bevacqua, A. N. Cranin, D. Whittlesey, Academic Press, London, 415–420, 1996

[14]. M. Baciut, G. Baciut, V. Simon, C. Albon, V. Coman, P. Prodan, St. I. Florian, S. Bran, J. Optoelectr. Adv. Mat., 9, 2547, 2007.

[15]. M. Goldman, L. Pruitt, J. Biomed Mater Res., 40, 378, 1998.

[16]. E. M. Noah, J. Chen, X. Jiao, I. Heschel, N. Pallua, Biomaterials. 23, 2855, 2002.

[17]. M. Takechi, Y. Miyamoto, Y. Momota, T. Yuasa, S. Tatehara, M. Nagayama, K. Ishikawa, J. Biomed. Mater. Res. B Appl Biomater., 69, 58, 2004.

[18]. S. Lerouge, C. Guignot, M. Tabrizian, D. Ferrier, N. Yagoubi, L. Yahia, J. Biomed. Mater. Res., 52, 774, 2000.

[19]. P. D. Nair, J. Biomater. Appl., 10, 121, 1995.

[20]. R. Gref, A. Domb, P. Quellec, T. Bunk, R. H. Muller, J. M. Verbavatz, R. Langer, Advanced Drug Delivery reviews, 16, 215 – 233, 1995.

[21]. C. C. Berry, S. Adams, G. Curtis, *J. Phys. D: Appl. Phys.* 36, 198- 206, 2003.

[22]. L. Tang, A.H. Lucas, J.W. Eaton, J Lab Clin Med; 122(3): 292-300, 1993.

[23]. L. Tang L, J. W. Eaton, Am J Clin Pathol; 103(4): 466-71, 1995.

[24]. V. Balasubramanian *et al*., J Biomed Mater Res; 44(3): 253-60, 1999.

[25]. D.L. Griscom, Science and Technology, Eds. G. Pacchioni, L. Skuja and D.L. Griscom, Kluwer Academic Publishers, p. 117, 2000.

[26]. S.H. Hyun, S.C. Yi, S. G.Kim, J Mat Sci Lett; 15:1384-1387, 1996.

[27]. F. He, W.T. Petuskey, Mater Lett; 63:2631-2634, 2009.

[28]. Y. Sun, L. Duan, Z. Guo, Y. Duanmu, M. Ma, L. Xu, et al., J Magn Magn Mater;285:65-70, 2005.

[29]. V. Simon et al., J. Non-Cryst. Solids 351, 2365-2372, 2005.

[30]. D. Cacaina, H. Ylänen, D. A. Udvar, S. Simon, J. Optoelectr. Adv. Mater., 9, 675, 2007.

[31]. A. Arvidsson, F. Currie, P. Kjellin, Y.T. Sul, V. Stenport, J Mater Sci: Mater Med; 20:1869-1879, 2009.

[32]. S.L. McArthur, Surf Interface Anal; 38:1380–1385, 2006.

[33]. M. Advincula M, Fan X, Lemons J, Advincula R, Colloid Surface B;42:29-43, 2005.

[34]. A. P. Serro, M.P. Gispert, M.C.L. Martins, P. Brogueira, R. Colaco, B. Saramago, J Biomed Mater Res;78A:581-589, 2006.

[35]. A. Lebugle, M. Subirade, J. Gueguen, BBA Protein Struct Mol Enzymol; 1248:107-114, 1995.

[36]. D.D. Deligianni, N. Katsala, S. Ladas, Sotiropoulou D, Amedee J, Missirlis YF, Biomaterials; 22:1241-1251, 2001.

[37]. G. Speranza, M. Ferrari, M. Bettinelli, Philos Mag B; 79:2145-2155, 1999.

[38]. G. Iucci, G. Polzonetti, G. Infante, L. Rossi, Surf Interface Anal; 36:724-728, 2004.

[39]. G. Reiter, N. Hassler, V. Weber, D. Falkenhagen, U.P. Fringeli, Biochim. Biophys. Acta 1699, 253-261, 2004.

[40]. G. Falini, E. Foresti, I.G. Lesci, B. Lunelli, P. Sabatino, N. Roveri, Chem. Eur. J. 12, 1968-1974, 2006.

[41]. W.J. Yang, P.R. Griffiths, D.M. Byler, H. Susi, Appl. Spectrosc. 39, 282-287,1985.

[42]. D.M. Byler, H. Susi., Biopolymers **25**, 469-487, 1986.

[43]. C.K. Krishnan, Biomaterials 19, 357-369, 1998.

[44]. S. Tunc, M.F. Mainz, G. Steiner, L. Vazquez, M.T. Pham, R. Salzer, Colloid Surface B: Biointerfaces 42, 219-225, 2005.

[45]. K. K. Chittur, Biomaterials 19, 357-369, 1998.

[46]. F. Yi, Q. Li, Z.X. Guo, J. Yu, J. Appl. Polymer Sci. 99, 1340, 2006.

[47]. A. Asatekin, S. Kang, M. Elimelech, A.M. Mayes, J. Membrane Sci. 298, 136, 2007.

[48]. T. L. Barr, S. Seal, J. Vac. Sci. Technol. A: Vac. Surf. Films 13, 1239, 1995.

[49]. F. Zhang, R.J. Gates, V.S. Smentkowski, S. Natarajan, B.K. Gale, R.K. Watt, M.C. Asplund, M.R. Linford, J. Am. Chem. Soc. 129, 9252, 2007.

[50]. M.A.Z. Ewiss, Phys.Chem. Glasses 39 (4), 236, 1998.

[51]. V. Simon, D. Muresan, A.F. Takács, M. Neumann, S. Simon, Solid State Ionics 178, 221, 2007.

Acknowledgements

My warmest thanks go to my supervisor, **Prof. Dr. Viorica Simon**, for the honor and privilege of being accepted to work in her research group. Her understanding, encouraging and personal guidance have provided a good basis for the present thesis.

Similarly, I would like to thank **Prof. Dr. Simion Simon** for useful discussions and good advices.

My sincere gratitude and thanks goes to my committee members for proofreading of the thesis: **Prof. Dr. Dumitru Luca** from A. Cuza University, Iasi; **Prof. Dr. Ing. Cătălin Popa** from Technical University, Cluj-Napoca; and to **Prof. Dr. Leontin David,** Babeş-Bolyai University for his trust and kindness over the past 8 years.

I also want to thank to all my colleagues who helped me, giving both technical and moral support.

I am very thankful to all my friends and people from scientific circle that helped me with different kind of measurements, technical and guiding materials, especially to Camelia Albon from Bielefeld University, Germany; Răzvan Adam from "Vrije Universiteit" Brussels, Belgium; and Raluca Marcu from "Istituto Europeo di Oncologia", Milan, Italy.

My acknowledgements go as well to **Prof. Bernard Gallez** and his research group for giving me the opportunity to perform for over one year a research internship at "Université Catholique de Louvain", Brussels, Belgium.

I thank my family, my parents Cornelia and Ioan Vanea, for educating me and guiding me to sciences, for unconditional support and encouragement to pursue my interests.

And in a very special way I thanks with all my heart to my dear and loving husband for the provided inspiration and energy.

Finally, I acknowledge the financial support of the World Federation of Scientists and CNCSIS.